NREL
NATIONAL RENEWABLE ENERGY LABORATORY

Structural Design Considerations for Tubular Power Tower Receivers Operating at 650°C

Preprint

Ty W. Neises, Michael J. Wagner, and Allison K. Gray

To be presented at the 8th International Conference on Energy Sustainability
Boston, Massachusetts
June 30 – July 2, 2014

NREL is a national laboratory of the U.S. Department of Energy
Office of Energy Efficiency & Renewable Energy
Operated by the Alliance for Sustainable Energy, LLC

This report is available at no cost from the National Renewable Energy Laboratory (NREL) at www.nrel.gov/publications.

Conference Paper
NREL/CP-5500-61848
April 2014

Contract No. DE-AC36-08GO28308

This report is available at no cost from the National Renewable Energy Laboratory (NREL) at www.nrel.gov/publications.

Available electronically at http://www.osti.gov/scitech

Available for a processing fee to U.S. Department of Energy and its contractors, in paper, from:

U.S. Department of Energy
Office of Scientific and Technical Information
P.O. Box 62
Oak Ridge, TN 37831-0062
phone: 865.576.8401
fax: 865.576.5728
email: mailto:reports@adonis.osti.gov

Available for sale to the public, in paper, from:

U.S. Department of Commerce
National Technical Information Service
5285 Port Royal Road
Springfield, VA 22161
phone: 800.553.6847
fax: 703.605.6900
email: orders@ntis.fedworld.gov
online ordering: http://www.ntis.gov/help/ordermethods.aspx

Cover Photos: (left to right) photo by Pat Corkery, NREL 16416, photo from SunEdison, NREL 17423, photo by Pat Corkery, NREL 16560, photo by Dennis Schroeder, NREL 17613, photo by Dean Armstrong, NREL 17436, photo by Pat Corkery, NREL 17721.

Printed on paper containing at least 50% wastepaper, including 10% post consumer waste.

STRUCTURAL DESIGN CONSIDERATIONS FOR TUBULAR POWER TOWER RECEIVERS OPERATING AT 650°C

Ty W. Neises
NREL
Golden, CO, USA

Michael J. Wagner
NREL
Golden, CO, USA

Allison K. Gray
NREL
Golden, CO, USA

ABSTRACT

Research of advanced power cycles has shown supercritical carbon dioxide power cycles may have thermal efficiency benefits relative to steam cycles at temperatures around 500 - 700°C. To realize these benefits for CSP, it is necessary to increase the maximum outlet temperature of current tower designs. Research at NREL is investigating a concept that uses high-pressure supercritical carbon dioxide as the heat transfer fluid to achieve a 650°C receiver outlet temperature. At these operating conditions, creep becomes an important factor in the design of a tubular receiver and contemporary design assumptions for both solar and traditional boiler applications must be revisited and revised. This paper discusses lessons learned for high-pressure, high-temperature tubular receiver design. An analysis of a simplified receiver tube is discussed, and the results show the limiting stress mechanisms in the tube and the impact on the maximum allowable flux as design parameters vary. Results of this preliminary analysis indicate an underlying trade-off between tube thickness and the maximum allowable flux on the tube. Future work will expand the scope of design variables considered and attempt to optimize the design based on cost and performance metrics.

INTRODUCTION

One strategy to improve the electric conversion efficiency of a concentrating solar power (CSP) plant is to increase the hot-side temperature of the thermal power cycle. The power tower technology is considered one of the best options to achieve the temperatures required to realize high-efficiency utility-scale power cycle technologies. One common tower receiver design employs tubular panels that absorb incident flux and transfer the thermal power to a heat transfer fluid (HTF) – often molten salt [1] air [2], or steam [3]. The location and orientation of the tubes relative to supply headers, other tubes, inactive receiver walls, and the heliostat field is critical to the thermal efficiency of the receiver [4], [5]. Moreover, the design of the tube material, dimensions, and operating conditions impacts the operable lifetime of the tubes. This consideration is especially important for proposed high-temperature, high-pressure receivers where creep-fatigue behavior is significant.

Ongoing research at NREL is investigating the design and performance of a high pressure supercritical carbon dioxide (sCO_2) receiver as a means to achieve higher receiver HTF outlet temperatures [6]. Carbon dioxide is stable, environmentally benign, and behaves as a dense gas over the range of receiver operation (470-650°C, 20-25 MPa). Unlike steam, a carbon dioxide HTF operates as a single-phase fluid and therefore maintains more availability when interfaced with a sensible heat storage medium. This paper evaluates the structural design of a sCO_2 receiver tube with an operating pressure of 25 MPa, an inlet temperature of 470°C, and an outlet temperature of 650°C.

BACKGROUND

As a heat transfer medium, CSP receiver tubes are necessarily subject to a thermal gradient between the outer flux absorbing surface and the contained HTF. At steady-state, the heat transfer rate is proportional to the temperature difference and also to the thermally-induced stress across the wall. Besides a radial temperature gradient, receiver tubes are typically not uniformly heated in the circumferential and axial directions, and this uneven heating pattern leads to additional thermal stresses in the material. Furthermore, the fluid must contain a pressurized fluid, creating hoop and longitudinal stresses in the tubes. The design of the receiver must account for the stress from these various thermal and pressure gradients while maximizing operating temperature to enable efficient cycle operation.

A useful but incomplete analogy to the design of a high-pressure tubular CSP receiver is the design of a traditional (e.g. coal-fired) boiler and superheater. The primary differences between these cases are as follows:

1. CSP receivers necessarily operate diurnally and as a result experience significant cyclical behavior that can lead to fatigue failure.

2. CSP receivers, especially towers, are often designed to maximize flux concentration and minimize the surface area required for a given thermal-power rating, thereby reducing the surface area available to lose heat to the environment.

In contrast, the highest temperature regions in a traditional boiler/superheater are located in the superheater and typically are convectively heated by flue gas at relatively low rates of thermal flux. This convention has led to "worst-case" tube design guidelines that are targeted at superheater tubes experiencing lower rates of heat transfer.

Because of these differences, *ASME Boiler and Pressure Vessel Code, Section I: Rules for Construction of Power Boilers* [7] is inadequate for the complete design of high-flux CSP receivers. One proposed alternative is to use *Section III Division 1 – Subsection NH: Rules for Construction of Nuclear Facility Components* which takes a more conservative tract and requires more detailed stress calculations specific to plant operating conditions and a creep-fatigue analysis. The drawback to this approach is that – because of the large safety factors – previous research has found the nuclear requirements too restrictive for CSP applications. Consequently, simplified design rules based on the nuclear code were developed for CSP receivers and documented in an interim design standard [8]. Notably, this standard provides guidelines for creep-fatigue analysis.

$$\sum_{j=1}^{p}\left(\frac{n}{N_d}\right)_j + \sum_{k=1}^{q}\left(\frac{t}{T_d}\right)_k \leq D \qquad (1)$$

The standard prescribes a cumulative creep-fatigue damage analysis. Equation (1) shows the general creep-fatigue damage equation for p – number of unique loading cycles, and q – number of unique creep loads, where N_d is the number of allowable and n is the number of applied cycles at known loading cycle j, T_d is the allowable creep rupture time and t is the applied load time at loading condition k. Grossman et al. [9] highlight that this creep-fatigue analysis is based entirely on empirical data and not on the physical processes leading to creep-fatigue failure. Therefore D varies for different materials and should be found using measured data. Reference material for Haynes 230 suggests that its D is around or greater than one [10].

One difficultly with Equation (1) is that it requires knowledge of the receiver's operating conditions over its lifetime. Kistler [11] suggests that for Barstow, California the fatigue damage to a molten salt receiver caused by 30 years of operation can be approximated by evaluating 10,000 equivalent design cycles. Ideally, this calculation would be repeated for each climate and receiver design permutation, but it provides a good starting point for high-level analyses. A similar analysis should be completed to determine the equivalent hours at the design conditions that approximate the damage caused by entire receiver lifetime. Instead the following analysis assumes 100,000 hours, which is roughly equal to the design conditions operating nine to ten hours per day over 30 years. This is likely a conservative approximation given the number of non-operational cloudy days in even the sunniest climates.

Many receiver design studies have been published in the past four decades. Most of these studies focus on either steam or molten salt receivers at temperatures less than 600°C using established engineering alloys and available computational techniques. These studies have generally chosen to ignore creep affects for several reasons; namely, lower operational temperatures inhibit creep damage, and relatively larger compressive thermal stresses outweigh smaller tensile pressure stresses at the high temperature locations in the tube (outer surface). Consequently, receiver tube design studies that simultaneously consider high temperature, high pressure, and non-uniform radial and circumferential thermal gradients in thick-walled tubes have not been presented.

NOMENCLATURE

Cumulative creep-fatigue parameters: Eq. (1)	
D	Maximum allowable cumulative creep-fatigue
j	Known loading cycle
k	Known load condition
n	Number of applied loading cycle at j
N_d	Number of allowable loading cycles at j
p	Number of unique loading cycles
q	Number of unique creep loads
T	Total applied load time at k
T_d	Allowable creep rupture time at k
Stress and strain calculations	
E	Modulus of Elasticity
$S.F.$	Safety Factor
p_i	Internal pressure
r_i	Inner radius
r_o	Outer radius
α	Thermal expansion coefficient
ε	Strain
v	Poisson's ratio
σ_r	Stress in the radial direction
σ_l	Stress in the longitudinal direction
σ_θ	Stress in the tangential direction
ΔT	Temperature difference

APPROACH

Calculating receiver lifetime requires calculation of the stresses resulting from internal tube pressure and temperature gradients. In this analysis the flux is assumed to be uniform around the circumference of the tube. Furthermore, thermal stresses caused by axial temperature differences are ignored. This approach sets an upper bound on the maximum allowable flux and allows meaningful comparison with traditional superheater designs. Thermal-fluid calculations were completed using Engineering Equation Solver (EES) [12], which contains carbon dioxide property data and appropriate thermo-fluids correlations. Because of the small diameters and high Reynolds number flow used in this study, the model assumed fully developed turbulent flow.

The stresses in the tube wall can be calculated in the three principal directions: radial (r), tangential (θ, this stress is

commonly referred to as the hoop stress when it's caused by internal pressure), and longitudinal (l). Because the ratio of inner radius to tube thickness is less than 10, thick-wall calculations must be used rather than the more common thin wall calculations. Equations (2), (3), and (4) show the pressure stresses as a function of radial position.

$$\sigma_r = \frac{p_i r_i^2}{r_o^2 - r_i^2}\left(1 - \frac{r_o^2}{r^2}\right) \quad (2)$$

$$\sigma_\theta = \frac{p_i r_i^2}{r_o^2 - r_i^2}\left(1 + \frac{r_o^2}{r^2}\right) \quad (3)$$

$$\sigma_l = \frac{p_i r_i^2}{r_o^2 - r_i^2} \quad (4)$$

Thick-wall calculations are also required to calculate the stresses resulting from the radial temperature difference through the tube wall and are shown in Equations (5),(6), and (7) [13]. The temperature difference (ΔT) is calculated as the inner wall temperature minus the outer wall temperature. Thermal and pressure stresses are superimposed to find the total stress in each principal direction.

$$\sigma_r = \frac{\alpha E \Delta T}{2(1-\nu)\ln\left(\frac{r_o}{r_i}\right)}\left[-\ln\frac{r_o}{r} - \frac{r_i^2}{r_o^2 - r_i^2}\left(1 - \frac{r_o^2}{r^2}\right)\ln\left(\frac{r_o}{r_i}\right)\right] \quad (5)$$

$$\sigma_\theta = \frac{\alpha E \Delta T}{2(1-\nu)\ln\left(\frac{r_o}{r_i}\right)}\left[1 - \ln\frac{r_o}{r} - \frac{r_i^2}{r_o^2 - r_i^2}\left(1 + \frac{r_o^2}{r^2}\right)\ln\left(\frac{r_o}{r_i}\right)\right] \quad (6)$$

$$\sigma_l = \frac{\alpha E \Delta T}{2(1-\nu)\ln\left(\frac{r_o}{r_i}\right)}\left[1 - 2\ln\frac{r_o}{r} - \frac{2r_i^2}{r_o^2 - r_i^2}\ln\left(\frac{r_o}{r_i}\right)\right] \quad (7)$$

Table 1: Parameters for example of pressure and thermal stresses.

Parameter	*Value[units]*
O.D. / Thickness	12 / 2 [mm]
I.D / O.D Temperatures	666.3 / 676.9 [°C]
Pressure	25 [MPa]
E (modulus of elasticity)	1.7 x 10^5 [MPa]
α (thermal expansion coef.)	1.67 x 10^{-5} [1/°C]
ν (Poisson's ratio)	0.31 [-]

Table 1 lists example values from the next section to demonstrate the stress equations; the results are plotted in Figure 1. The plot shows that the maximum stress in the tube is caused by the pressure hoop stress and is located on the inner surface of the tube. Combined with the tangential thermal stress, the total tangential stress at the inner surface is the largest principal stress in the tube. It is also notable that the both the tangential and longitudinal total stresses are tensile and greater at the inner radius than the outer radius. Although the temperature is hottest at the outer surface, the inner surface may also experience creep due to the high fluid exit temperature, so this analysis calculates the creep-fatigue damage at both the inner and outer radii.

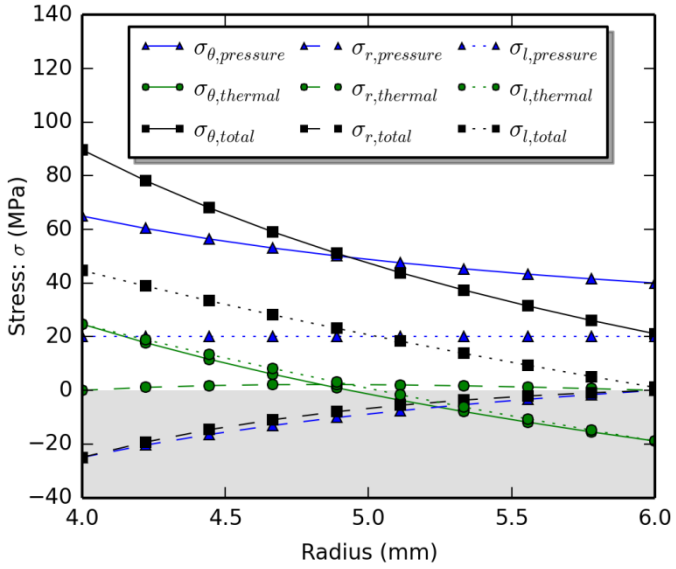

Figure 1: Pressure, thermal, and total stresses in the radial, tangential, and longitudinal directions, using parameters from Table 1.

Next both the fatigue and creep sections of the creep-fatigue analysis must be completed. The fatigue damage is calculated using the strain in the receiver tube. First, the calculated strain is multiplied by 1.1 to approximate the inelastic strain [14]. The equivalent strain is then calculated using Equation (8) where the subscripts correspond to the three principal directions, multiplied by a safety factor of 2.0 [15], and then used to calculate the number of allowable cycles. Finally, the number of design cycles (10,000) is divided by the calculated number of allowable cycles to predict the fatigue damage. As a final safety factor, the minimum fatigue damage in the following analysis is also limited to 0.1.

$$\varepsilon_{equiv} = \frac{\sqrt{2}}{3}\sqrt{\{(\varepsilon_1 - \varepsilon_2)^2 + (\varepsilon_1 - \varepsilon_3)^2 + (\varepsilon_3 - \varepsilon_2)^2\}} \quad (8)$$

Creep damage is also calculated using predicted receiver material temperatures and stresses. The maximum principal stress (σ_{max}) can be used for materials for which tensile stress governs creep rupture. (It is assumed here that tensile stress governs creep rupture in Haynes 230, however this assumption must be verified.) The calculated maximum tensile stress is multiplied by a safety factor (S.F.) of 1.5 in concordance with the Maximum Allowable Stress values in the BPVC, and this value is used to calculate the creep rupture lifetime. Finally, the total number of hours at design conditions (100,000, as discussed above) is divided by the calculated time to creep rupture to calculate the predicted creep damage.

Table 2 shows the calculated equivalent strain, maximum principal stress, fatigue and creep damages, and total damage for both the inner and outer tube surfaces. The larger maximum principle stress and sufficiently high temperature on the inner surface is enough to induce creep damage and act as the limiting design consideration for this configuration. An increase in the radial temperature gradient compared to the Table 2

analysis would result in a total damage greater than one and lead to potential tube failure before its targeted 30 year lifetime.

Table 2: Calculated lifetime metrics for the inner and outer tube surfaces for the example tube pressure and thermal profile described in Table 1.

Calculated Value	*Units*	*Inner*	*Outer*
$\varepsilon_{equiv} *$ Safety Factor	%	0.086	0.018
Number of allowable cycles	-	100,000+	100,000+
Fatigue Damage	-	0.1	0.1
$\sigma_{sigma} *$ Safety Factor	MPa	133.6	31.72
Time to creep rupture	Hours	111588	1E8
Creep Damage	-	0.8962	0.001
Total Damage	-	0.9962	0.101

RESULTS

The following analysis employs the approach outlined in the previous section to investigate the maximum allowable flux intensity on the receiver as a function of the local internal HTF temperature and selected tube wall thickness. In other words, given an absorber tube diameter and wall thickness, we seek to demonstrate the maximum allowable flux that can be absorbed at any point along the flow path. This knowledge aids in the design of the absorber, selection of a suitable flow path, configuration of the receiver geometry, and definition of a heliostat field aiming strategy.

Performance was evaluated at the design and operational conditions listed in Table 3. The target inlet and outlet temperatures and operating pressure were selected from a hypothetical high-efficiency, partial-cooling sCO_2 cycle [16]. The tube diameter, length, and heat absorbed are representative values that balance pressure drop, material usage, and receiver thermal and optical efficiency. Haynes 230 was selected as the material because it is commercially available and has a comparatively high allowable stress at the desired operating conditions. Haynes International, Inc. [17] provided creep and fatigue data for this study.

Table 3: Parameters used for maximum flux analysis

Parameter	*Value[Units]*
Inlet Temperature	470 [°C]
Outlet Temperature	650 [°C]
Operating Pressure	25 [MPa]
Tube Diameter	1.2 [cm]
Tube Roughness	0.045 [mm]
Tube Length	4.1 [m]
Tube Thickness	*parametric* [mm]
Min/Max Thickness	1.4/3.6 [mm]
Heat Absorbed	14.76 [kW]
Max Flux	*parametric* [kW/m^2]

The results of this analysis depend strongly on the assumed tube dimensions, including wall thickness. Our study determined wall thickness for a given tube outer diameter by considering both absorber lifetime and pressure loss through the receiver along the flow path. First, we calculate a minimum thickness required to achieve the desired receiver lifetime at the outlet temperature assuming no heat transfer through the tube. Then the modeled thickness is increased until the simulated pressure drop exceeds 5% of the total turbine inlet pressure value. For the conditions in Table 3, this results in a maximum thickness of 3.6 mm and a pressure drop equal to 5.6%. The calculations assume an average absorbed flux (independent of the local maximum flux) and a corresponding HTF mass flow rate to maintain an outlet temperature of 650°C. Therefore, given the constant outer tube diameter, the pressure loss through the receiver is strictly dependent on tube thickness.

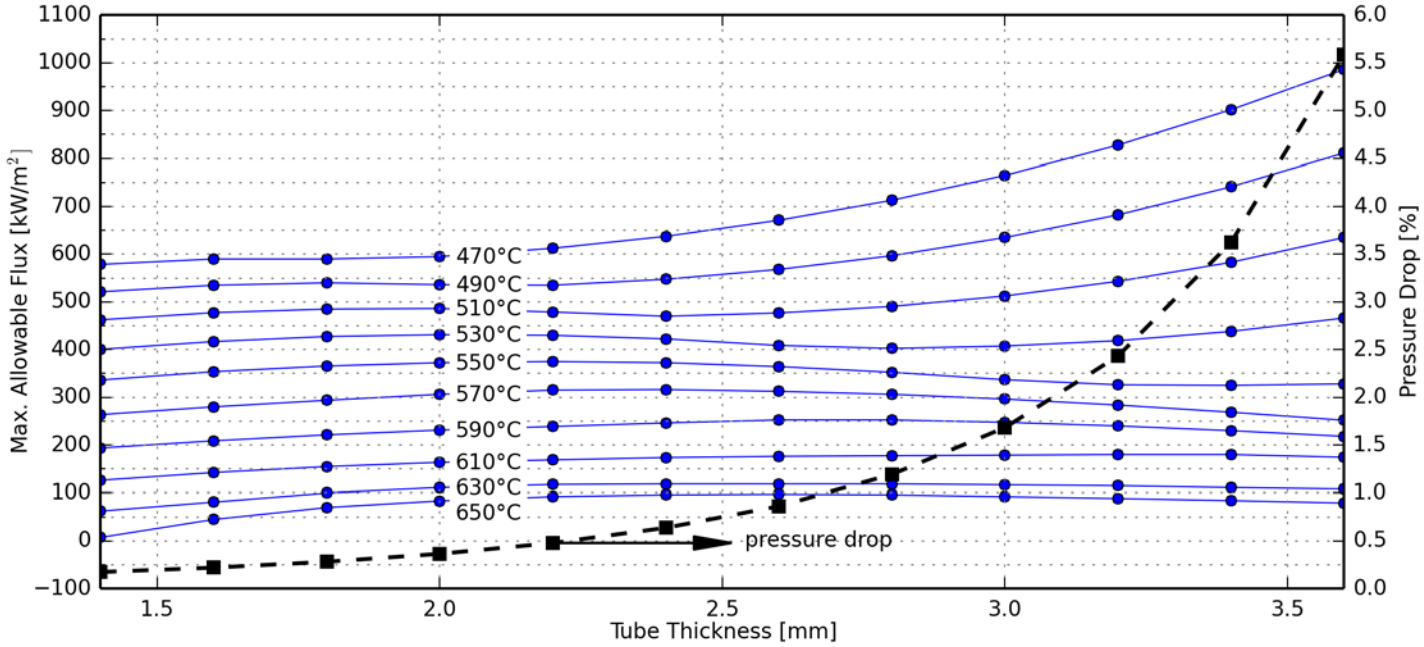

Figure 2: Maximum allowable flux and pressure drop as a function of thickness for different temperatures in sCO2 flow path. The flux is assumed uniform around the circumference of the tube.

After identifying the range of feasible thickness values, the maximum allowable flux was calculated for each thickness across the range of design inlet to outlet temperatures. The pressure was fixed at the (higher) receiver inlet pressure. Figure 2 maps the of maximum flux value alongside the pressure drop for each tube thickness. The plot shows that as fluid temperature changes, the maximum-flux thickness also varies.

The benefit of increasing thickness is maximized at the hottest fluid temperatures, although this advantage quickly plateaus for the 650°C fluid temperature above a thickness of around 2 mm. This particular thickness also limits the pressure drop to less than 1% and corresponds to allowable flux levels close to the maximum flux at decreasing temperatures until around 500°C, below which very thick tubes can increase the maximum allowable flux by around 50%, albeit with higher associated pressure drops.

Figure 3 investigates tube damage as a function of temperature at 2 mm wall thickness and tube damage as a function of wall thickness at the maximum temperature of 650°C. The figure shows that creep damage on the inner surface constrains the maximum allowable flux on the tube. The damage from inner surface fatigue is limited to the minimum value we assign, 0.1. The outer surface fatigue behaves similarly, while the creep damage from the outer surface is negated by coinciding compressive thermal stresses. One minor but noteworthy exception is for creep damage at the hottest fluid temperature and smallest tube thickness - approximately 0.1. This result is caused by a lack of compressive thermal stresses to counterbalance the tensile pressure stresses. Creep damage on the inner surface governs the maximum allowable flux and the creep is controlled by the maximum tensile stress. Thus, the maximum tensile stress at the inner surface - composed of the sum of the pressure and thermal stresses - drives the maximum allowable flux.

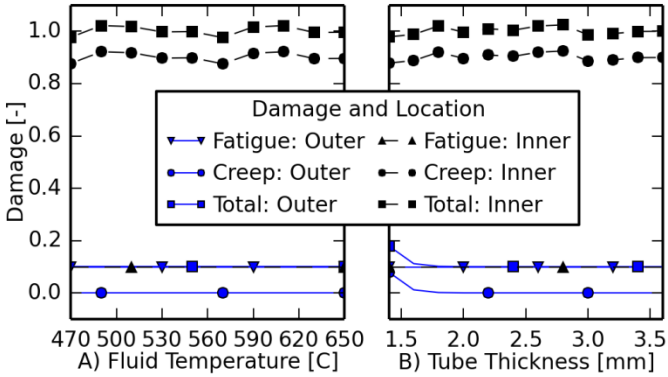

Figure 3: Fatigue, creep, and total damage for the parameters in Table 3 at the maximum flux conditions for A) a thickness of 2 mm for varying fluid temperatures and B) varying fluid thickness at the outlet temperature. The variance in creep and total damages for the inner surface is caused by the tolerance used to find the maximum flux.

Figure 4 shows the interaction between tensile stresses, maximum flux, and tube thickness at a fluid temperature of 650°C. When the tube thickness is increased for a given flux, three responses are observed:

1. The pressure stress decreases.
2. The thermal stress in the tube wall increases.
3. The inner surface temperature decreases because the convection coefficient increases due to increased fluid velocity.

Conversely, as the flux is increased for a given wall thickness, the thermal stress in the tube wall and the inner wall temperature also increase, leading to lower allowable stress values. The interaction between these effects determines the maximum allowable flux at each thickness.

Figure 4 shows that as the thickness increases from its minimum value, pressure stress decreases, enabling an increase in maximum allowable flux. Eventually, the pressure decrease slows while the tube temperature and thermal stresses increase.

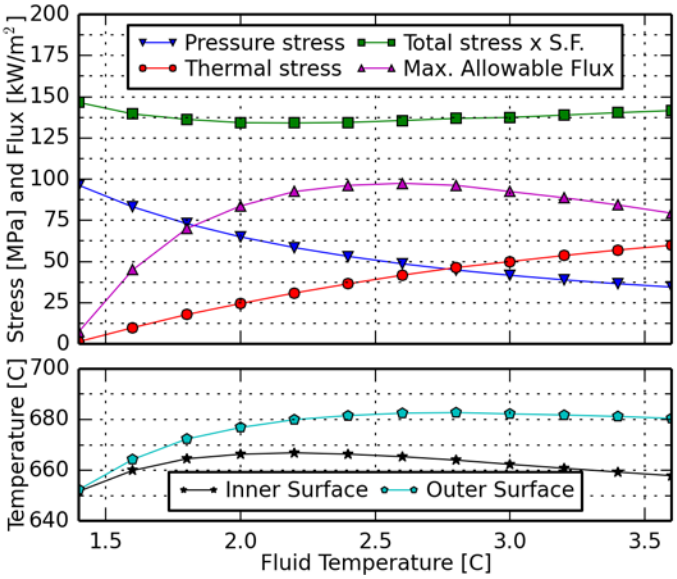

Figure 4: Tangential stresses at the inner surface and maximum allowable flux as a function of tube thickness for a fluid temperature of 650°C.

Figure 5 shows the interaction between tensile stresses, maximum flux, and fluid temperature at a tube wall thickness of 2 mm. Because the wall thickness, fluid pressure, and heat transfer coefficient are constant, the pressure stress is constant. Therefore, the allowable thermal stress at each fluid temperature is only a function of the tube temperature and flux. For a given fluid temperature, the flux is increased until the sum of the constant pressure stress and the thermal stress is equal to the allowable stress at the tube temperature. The tube temperature increases as the flux increases, and as a result the allowable stress due to creep rupture life decreases.

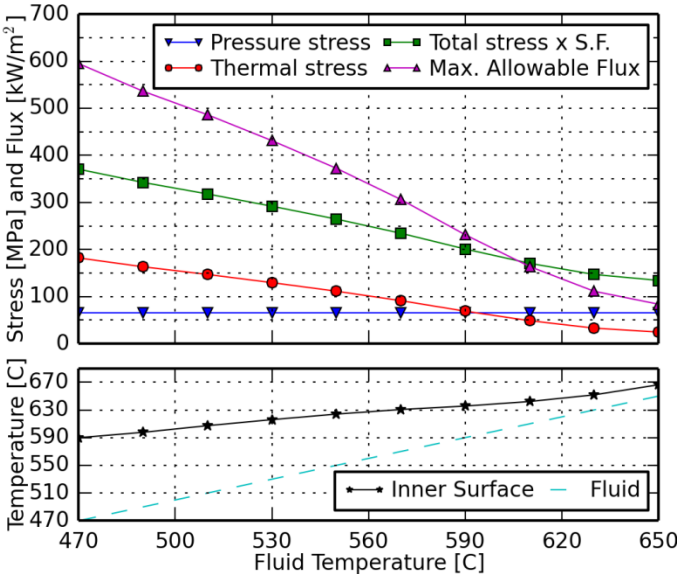

Figure 5: Tangential stresses at the inner surface and maximum allowable flux as a function of fluid temperature for a tube thickness of 2 mm.

CONCLUSIONS

This paper employs a cumulative creep-fatigue analysis to consider a high-pressure, high-temperature sCO_2 receiver tube for 10,000 design cycles and 100,000 design hours. In contrast to steam and molten salt receiver designs running at lower temperature and/or pressure, these conditions can lead to significant creep damage on the inner tube surface due to the superposition of tensile pressure and tensile thermal stresses. The hotter outside surface experiences a counteracting superposition of tensile pressure and compressive thermal stresses.

Results of a simplified uniform flux analysis show that, for a given fluid temperature, an optimum tube wall thickness may exist that yields a unique maximum allowable flux. This optimum balances decreasing pressure stress, increasing thermal stress, and potentially decreasing (depending on inner surface temperature) allowable stress with increasing thickness. It follows that for a given thickness, the maximum allowable flux increases as the fluid temperature decreases.

This study provides an initial review of driving factors in the design of a high pressure, high temperature receiver, and it highlights some important design differences compared to existing CSP receiver technologies. However, the effect of simplifications in this preliminary analysis must be noted and studied further. Most importantly, circumferential flux variation may introduce additional thermal stress and must be quantified. Non-uniform flux may significantly decrease the maximum allowable flux presented in this study. This effect will be proportionally more significant at high temperatures. Internal tube surface corrosion over its lifetime may also negatively affect the maximum allowable flux. Issues regarding transient operation, startup and shutdown, and weld strength at up- and down-stream headers must be considered in a similar lifetime analysis. Finally, this approach might be applied to a wider range of design parameters (e.g. tube diameter, average absorbed thermal power) to provide meaningful design optimization.

ACKNOWLEDGMENTS

This work was supported by the U.S. Department of Energy under Contract No. DE-AC36-08-GO28308 with the National Renewable Energy Laboratory.

REFERENCES

[1] W. R. Gould, “SOLARRESERVE’S 565 MWt MOLTEN SALT POWER TOWERS,” in *Proceedings of the 2011 SolarPACES International Symposium*, pp. 1–5.

[2] “SOLGATE - Solar hybrid gas turbine electric power system,” European Commission, Luxembourg, 2005.

[3] D. Fernández, “PS10: a 11-MWe Solar Tower Power Plant with Saturated Steam Receiver.” 2004.

[4] M. J. Wagner, “Simulation and Predictive Performance Modeling of Utility-Scale Central Receiver System Power Plants by,” University of Wisconsin - Madison, 2008.

[5] M. R. Rodríguez-Sánchez, A. Soria-Verdugo, J. A. Almendros-Ibáñez, A. Acosta-Iborra, and D. Santana, “Thermal design guidelines of solar power towers,” *Appl. Therm. Eng.*, vol. 63, no. 1, pp. 428–438, Feb. 2014.

[6] U.S. Department of Energy, “SunShot Initiative: Direct Supercritical Carbon Dioxide Receiver Development,” 2013. [Online]. Available: http://www1.eere.energy.gov/solar/sunshot/lab_nrel_receiver.html.

[7] *ASME Boiler and Pressure Vessel Code*. New York, NY: American Society of Mechanical Engineers, 2011.

[8] I. Berman, A. C. Gangadharan, G. D. Gupta, and T. V. Narayanan, “An Interim Structural Design Standard for Solar Energy Applications.pdf,” Sandia National Laboratories, Livermore, CA, Report No. SAND79-8183, 1979.

[9] J. W. Grossman, W. B. Jones, and P. S. Veers, “Evaluation of Thermal Cycling Creep-Fatigue Damage for a Molten Salt Receiver,” in *12th Annual ASME International Solar Energy Conference*, 1990.

[10] X. Chen, M. a. Sokolov, S. Sham, D. L. Erdman III, J. T. Busby, K. Mo, and J. F. Stubbins, “Experimental and modeling results of creep–fatigue life of Inconel 617 and Haynes 230 at 850°C,” *J. Nucl. Mater.*, vol. 432, no. 1–3, pp. 94–101, Jan. 2013.

[11] B. L. Kistler, “Fatigue Analysis of a Central Receiver Design Using Measured Weather Data,” Livermore, CA, 1987.

[12] “Klein, S.A. (2010). EES – Engineering Equation Solver, F-Chart Software. http://www.fchart.com.,” p. 2010, 2010.

[13] S. Timoshenko and J. N. Goodier, *Theory of Elasticity*. McGraw-Hill, 1951, p. 500.

[14] T. V. Narayanan, M. S. M. Rao, and G. Carli, “Structural Design and Life Assessment of a Molten Salt Solar Receiver,” *J. Sol. Energy Eng.*, vol. 107, pp. 258–263, 1985.

[15] D. C. Smith, “DESIGN AND OPTIMIZATION OF TUBE-TYPE RECEIVER PANELS FOR MOLTEN SALT APPLICATION,” *ASME J. Sol. Eng.*, vol. 2, 1992.

[16] T. Neises and C. Turchi, “A comparison of supercritical carbon dioxide power cycle configurations with an emphasis on CSP applications,” in *Proceedings of the 2013 SolarPACES International Symposium*, 2013.

[17] “Haynes International, Inc.” [Online]. Available: http://www.haynesintl.com/.